THE JOURNAL OF PHYSICAL CHEMISTRY C

C: Surfaces, Interfaces, Porous Materials, and Catalysis

Electrochemical Detection of *Pseudomonas Aeruginosa* Quorum Sensing Molecules at a Liquid|Liquid Interface

Edward D. Burgoyne, Talia Jane Stockmann, Andrés F. Molina-Osorio, Rachel Shanahan, Gerard P. McGlacken, and Micheál D. Scanlon

J. Phys. Chem. C, **Just Accepted Manuscript** • DOI: 10.1021/acs.jpcc.9b08350 • Publication Date (Web): 12 Sep 2019

Electrochemical Detection of *Pseudomonas aeruginosa* Quorum Sensing Molecules at a Liquid|Liquid Interface

Edward D. Burgoyne,[†] Talia Jane Stockmann,[‡,*] Andrés F. Molina-Osorio,[†] Rachel Shanahan,[§] Gerard P. McGlacken,[§] and Micheál D. Scanlon[†, ‖,*]

[†] The Bernal Institute and Department of Chemical Sciences, School of Natural Sciences, University of Limerick (UL), Limerick V94 T9PX, Ireland

[‡] Memorial University of Newfoundland, Chemistry Department, 283 Prince Philip Dr. St. John's, NL Canada A1B 3X7

[§] School of Chemistry and Analytical and Biological Chemistry Research Facility, University College Cork, College Road, Cork, Ireland

[‖] Marine and Renewable Energy Ireland (MaREI) Centre

ABSTRACT: Opportunistic pathogenic bacteria, such as *Pseudomonas aeruginosa*, pose a serious risk to patients suffering from a compromised immune system and those patients with cystic fibrosis. Confirming their presence often requires culturing the bacteria which can take days. Herein is proposed a rapid electrochemical detection method based on *P. aeruginosa* generated small molecules employed for chemical communication – referred to as quorum sensing (QS) molecules – within the biofilm formed by the bacteria; specifically, 4-hydroxy-2-heptylquinoline (HHQ) and 2-heptyl-3,4-dihydroxyquinoline (PQS, Pseudomonas quinolone signal). This method does not depend on the redox activity of the QS molecules. Instead, as a proof-of-concept, electrochemical monitoring was achieved through aqueous alkali metal ion and proton interfacial complexation with organic solubilized HHQ and PQS at an interface between two immiscible electrolytic solutions (ITIES), specifically, between water and 1,2-dichloroethane. The proton:HHQ and proton:PQS binding stoichiometry's were discovered to be 1:3 and 1:2, respectively, which is likely due to the relatively high concentrations of QS molecules employed. Owing to the biphasic nature of the methodology, experimental complications due to the poor solubility of the hydrophobic QS molecules in aqueous media were avoided.

Introduction

Rapid detection, monitoring, and identification of pathogenic bacteria allows for equally fast application of treatment measures minimizing adverse health effects of at-risk-patients, *e.g.*, those with compromised immune systems. At the same time, increased fundamental understanding of cell-to-cell communication which bacteria achieve through small molecules, referred to as quorum sensing (QS), can guide the development of point-of-care-devices.[1-3] Indeed, an increasing number of small signalling molecules have been identified[1] that bacterial colonies use for cooperation in a pseudo-multicellular fashion that regulate gene expression in the local bacterial population or colony.[4-7] Exploiting small molecules associated with QS for bacterial monitoring is advantageous, particularly in light of an increasingly antibiotic resistant paradigm[7-9] where early recognition is key to patient treatment success.[10]

Pseudomonas aeruginosa (*P. aeruginosa*) is a Gram-negative bacteria and human pathogen that is responsible for a high number of hospital infections and is prevalent in patients with compromised immune systems, chronic wounds, and in the lungs of those suffering from cystic fibrosis.[11,12] Several redox active phenazine derivatives 2-alkyl-4-quinolones (AHQs) have been identified that behave as QS molecules produced by *P. aeruginosa*; *e.g.*, 4-hydroxy-2-heptylquinoline (HHQ) and 2-heptyl-3,4-dihydroxyquinoline (PQS, Pseudomonas quinolone signal, see Figure 1 for chemical structures).[2,7,9,10,13-32] AHQs exist in another tautomeric form and can also be termed 4-hydroxy-2-alkylquinolines (HAQs).[33] The neutral 4-quinolone rather than the 4-hydroxy-quinoline is the predominant species in the pH range 4–6.[34] Some small QS molecules – like pyocyanin – also act as virulence factors.

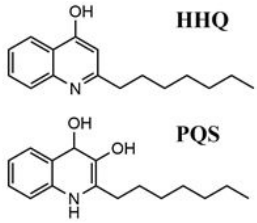

Figure 1. Chemical structures of 4-hydroxy-2-heptylquinoline (HHQ) and 2-heptyl-3,4-dihydroxyquinoline (PQS, Pseudomonas quinolone signal).

By exploiting their redox activity, electrochemical methods have been employed as rapid, high-throughput detection schemes to monitor HAQ production throughout the growth cycle of the biofilm.[9,10,14,15,18,19,21,24-31,35-37] Bellin *et al.*[24,30] employed an integrated circuit design

incorporating a 1824 micro-electrode array (each square-shaped micro-electrode was 100×100 μm) over an 8×8 mm area in order to electrochemically and spatiotemporally image the biofilm surface. A similar approach was used by Simoska *et al*.[2] who generated a disc-shaped microelectrode array with diameters of 1.54 μm whilst also confirming the presence of metabolites through desorption and nano electrospray ionization mass spectroscopy. Scanning electrochemical microscopy has also been used to image and track the production of QS redox-active molecules throughout the growth cycle of a *P. aeruginosa* colony.[29] Most redox detection methods focus on pyocyanin, which evidence suggests is unique to *P. aeruginosa*,[14] and therefore provides a high degree of specificity. However, signal overlap of other redox active QS metabolites may be problematic for widespread application of this method.[19]

In this article, we present proof-of-concept experiments for a simple electrochemical method suitable to facilitate rapid and cost-effective detection of AHQs; in particular, PQS and HHQ, in cell-free culture (supernatant) extracts of *P. aeruginosa* and patient sputum samples. The detection principle is based on the generation of an electrochemical signal at an electrified aqueous-organic interface when HHQ or PQS are present in the organic phase. The experimental design takes advantage of two key properties of HHQ and PQS molecules, first their hydrophobicity and therefore propensity to easily extract to organic solvents,[33] and second their ability to chelate cations, for example as demonstrated previously with Fe^{3+}.[34] Experimental protocols used to detect HHQ and PQS from *P. aeruginosa* supernatant extracts or sputum samples of cystic fibrosis patients typically possess a liquid|liquid extraction step in the protocol to extract HHQ and PQS to an organic solvent. This is followed by an evaporation step and redissolution of the extract in a solvent or matrix tailored towards the final analytical procedure. Leipert *et al.*[38] employed dispersive liquid|liquid microextraction (DLLME) to extract PQS and HHQ from *P. aeruginosa* supernatant samples using a methanol/chloroform (1:1, v/v) organic phase, followed by evaporation and redissolution in an ionic liquid matrix optimized for matrix-assisted laser desorption/ionization (MALDI) mass spectrometry. Buzid *et al*.[23] extracted HHQ and PQS from cystic fibrosis patients samples twice with chloroform (1:2, v/v sputum sample:chloroform), followed by evaporation and redissolution in acetonitrile for electrochemical detection at a boron-doped diamond electrode. Thus, in principle, using an interface between two immiscible electrolytic solutions (ITIES) as the sensing element eliminates the need for the evaporation and redissolution steps.

Herein, the interfacial mechanism underlying the electrochemical detection method is described. Liquid|liquid electrochemistry is advantageous owing to its reproducibility and lack of surface defects as the interface is molecularly sharp by its very nature. Moreover, the liquid|liquid interface is also biomimetic;[39-41] the water|oil interface simulates to a degree the cell membrane. Electrodes immersed in either phase bias the potential which experiences a potential drop localized across the ITIES; *i.e.*, the potential difference between the aqueous (ϕ_w) and organic (ϕ_o) phase potentials results in a Galvani potential difference ($\phi_w - \phi_o = \Delta_o^w\phi$).[39-41] The biased potential pushes and pulls ions across the interface and current is measured as a function of this charge transfer analogous to electrons being transferred across a solid|liquid interface. Critically, this technique allows the detection of non-redox active species as well as facilitating ion transfer mechanisms.[42-47] In the latter for example, a hydrophobic ligand or ionophore stationed in the organic phase can coordinate to a metal ion or proton positioned in the aqueous phase and lower the energy barrier or the amount of applied potential required to illicit ion transfer.[39-45]

HHQ and PQS coordination with protons as well as alkali and alkali earth metal ions was quantified using well established analytical solutions for interfacial facilitated ion transfer.[43] This method provides a unique means for HHQ and PQS detection that is not dependent on their redox activity.

Experimental Section

All chemicals were used as received without further purification, unless otherwise indicated, with all aqueous solutions generated using high purity water (>18.2 MΩ cm) from a Millipore MilliQ filtration system. The organic solvent 1,2-dichloroethane (DCE, ≥99.8%) was received from Sigma-Aldrich. Lithium chloride (LiCl, ≥95%), sodium chloride (NaCl, ≥99%), potassium chloride (KCl, ≥99%), magnesium chloride ($MgCl_2$, ≥98%), lithium sulphate (Li_2SO_4, ≥99%), lithium citrate (Li_3(citrate), 97%), lithium hydroxide (LiOH, ≥98%), tetrabutylammonium perchlorate ($TBAClO_4$, ≥99%), and bis(triphenylphosphoranylidene)-ammonium chloride (BACl, 97%) were purchased from Sigma-Aldrich. Lithium tetrakis(pentafluorophenyl)borate etherate ($Li(Et_2O)_nTB$, >99%) was obtained from Boulder Scientific. BACl and $Li(Et_2O)_nTB$ were used to prepare the organic phase supporting electrolyte bis(triphenylphosphoranylidene)ammonium tetrakis(pentafluorophenyl)borate (BATB) by metathesis of the two salts in a solution of 2:1, methanol:water. The white precipitate was filtered and then recrystallized in acetone at ~4°C overnight.

4-hydroxy-2-heptylquinoline (HHQ) and 2-heptyl-3,4-dihydroxyquinoline (PQS, Pseudomonas quinolone signal) were synthesized as previously described by McGlacken *et al.*[48] HHQ and PQS were deemed analytically pure based on NMR analysis. All spectra were consistent with that previously published.[49]

All electrochemical experiments were performed using a Metrohm potentiostat in a 4-electrode configuration,[40] as described in detail elsewhere. The liquid|liquid interfacial surface area was determined to be ~1.53 cm^2. The electrolytic cells employed are detailed in Scheme 1. The potential was referenced to the transfer of ClO_4^-, taken to be –0.154 V,[50] unless otherwise noted.

$$\mathrm{Ag}\,|\,\mathrm{AgCl}\,|\,\underset{(aq)}{\text{10 mM LiCl}}\,\|\,\underset{(DCE)}{\text{X mM } L\text{, 5 mM BATB}}\,|\,\underset{(aq\sim ref.)}{\text{Sat. BACl, 10 mM LiCl}}\,|\,\mathrm{AgCl}\,|\,\mathrm{Ag} \qquad \text{[Cell 1]}$$

$$\mathrm{Ag}\,|\,\mathrm{AgCl}\,|\,\underset{(aq)}{\text{10 mM YY}}\,\|\,\underset{(DCE)}{\text{X mM HHQ, 5 mM BATB}}\,|\,\underset{(aq\sim ref.)}{\text{Sat. BACl, 10 mM LiCl}}\,|\,\mathrm{AgCl}\,|\,\mathrm{Ag} \qquad \text{[Cell 2]}$$

$$\mathrm{Ag}\,|\,\mathrm{AgCl}\,|\,\underset{(aq)}{\text{10 mM LiCl, EE mM HCl}}\,\|\,\underset{(DCE)}{\text{1 mM } L\text{, 5 mM BATB}}\,|\,\underset{(aq\sim ref.)}{\text{Sat. BACl, 10 mM LiCl}}\,|\,\mathrm{AgCl}\,|\,\mathrm{Ag} \qquad \text{[Cell 3]}$$

$$\mathrm{Ag}\,|\,\mathrm{AgCl}\,|\,\underset{(aq)}{\text{10 mM LiCl, YY mM LiOH}}\,\|\,\underset{(DCE)}{\text{1 mM } L\text{, 5 mM BATB}}\,|\,\underset{(aq\sim ref.)}{\text{Sat. BACl, 10 mM LiCl}}\,|\,\mathrm{AgCl}\,|\,\mathrm{Ag} \qquad \text{[Cell 4]}$$

Scheme 1. Electrolytic cells employed. In Cells 1 and 3, *L* was either 4-hydroxy-2-heptylquinoline (HHQ) or 2-heptyl-3,4-dihydroxyquinoline (PQS, Pseudomonas quinolone signal) added to the organic phase at concentrations of X varying from 10 μM to 1 mM. In Cell 2 various aqueous phase supporting electrolytes (YY) were used including KCl, NaCl, $MgCl_2$, Li_2SO_4, and lithium citrate (Li_3(citrate)). In Cell 3 and 4 EE=[HCl] and YY = [LiOH], respectively, and were used to vary the pH of the aqueous phase.

Results and Discussion

Figure 2 (dashed curve) depicts the cyclic voltammogram (CV) recorded using Cell 1 with no HHQ/PQS added to the organic phase and LiCl as the aqueous supporting electrolyte. The sharp increase in the current signal at positive potentials and sharp decrease at negative potentials marks the limits of the polarizable potential window (PPW) which is the result of transfer of supporting electrolyte ions: Li^+ from w (water)→o (oil) and TB^- from o→w at the positive end; Cl^- from w→o and BA^+ from o→w towards negative potentials.[51,52] After addition of 1 mM HHQ to the organic phase (solid line in Figure 2) two peak-shaped waves were observed on the forward and reverse scans with half-wave potentials ($\Delta_o^w\phi_{1/2}$) of –0.008 and 0.279 V (labelled as peak 1 and 2, respectively in Figure 2). Peak 1 possesses a highly asymmetric ratio between the forward ($j_{p,\mathrm{fwd}}$) and reverse ($j_{p,\mathrm{rev}}$) peak current densities; *i.e.*, $j_{p,\mathrm{fwd}} / j_{p,\mathrm{rev}} < 1$. As the scan rate was increased from 5 to 100 mV·s^{-1} the $j_{p,\mathrm{fwd}} / j_{p,\mathrm{rev}}$ ratio of peak 1 increased concomitantly such that at high scan rates (~100 mV·s^{-1}) the ratio is ~1 (see Figure S1 in the Electronic Supplementary Information, ESI). Peak 1 is hypothesized to be the facilitated ion transfer of H^+ from w→o through interfacial complexation with HHQ (see Figure 1) dissolved in the organic phase through eq. 1 below,

$$m\mathrm{H}^+_{aq} + n\mathrm{HHQ}_{org} \rightarrow n\text{H-HHQ}^+_{org} \qquad [1]$$

where *m* is the stoichiometry of protons, *n* is the stoichiometry of HHQ, and likely coordinates to the proton through the nitrogen's lone electron pair. Owing to the use of MilliQ purified water, the pH of the aqueous phase is ~5.5–6; therefore, the concentration of protons ($c_{H^+_{aq}}$) is ~10 μM and sufficient to generate a measurable ion transfer current. Owing to the relatively negative onset potential of peak 1, it is proposed that the asymmetry at low scan rates is owing to spontaneous proton facilitated ion transfer. The lower onset potential is directly related to the energy or driving force required to elicit ion transfer. Since the potential is slightly negative for a positive ion, one can conclude that this process is spontaneous although slow. In this way, protons in the vicinity of the ITIES would have already been depleted once the scan is initiated and at slow scan rates this results in a diminished peak current signal. HHQ likely has amphiphilic character and may aggregate at the ITIES, similar to phospholipids,[42] contributing to this effect. Overall, however, owing to the hydrophobicity of HHQ the facilitated proton transfer mechanism was considered as either transfer through interfacial ion complexation (TIC) or transfer followed by organic phase complexation (TOC).[43,53] Other mechanisms are possible but for simplicity only these two have been considered.

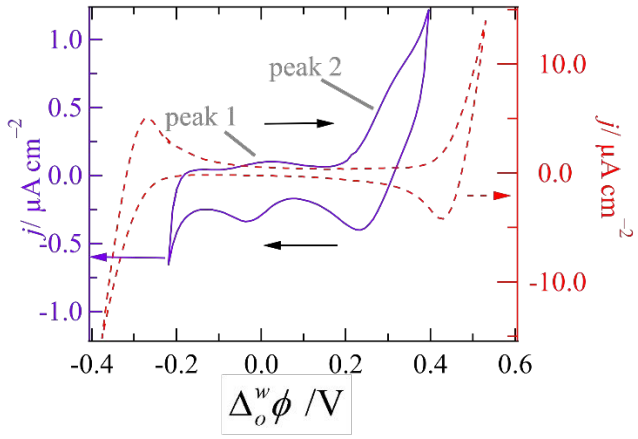

Figure 2. CVs acquired using Cell 1 without (dashed curve) or with 10 μM HHQ added to the organic phase (solid line). CVs were recorded at a scan rate (v) of 25 mV·s^{-1}.

If the aqueous phase supporting electrolyte is switched from LiCl to Li_3(citrate), then the H^+-HHQ facilitated ion peak is no longer visible (Figure 3, top panel) and likely owing to citrates relatively high basicity (pK_a's of citric acid are 3.13, 4.76, and 6.40)[54] meaning the doubly protonated state dominates at pH 5 (*i.e.*, AH_2^-, where A is the acid). In this case, citrate is behaving as a buffer and sequestering H^+ which in turn are not available to undergo eq. 1 above. This is confirmed by augmenting the pH of the aqueous phase, as discussed below. The PPWs for Li_3(citrate) (Figure 3, top panel) with and without HHQ added to the organic phase have positive potential limits of roughly 0.150 and 0.450 V, respectively. This is likely facilitated transfer of Li^+ by HHQ. Figure S2 (see ESI) shows a plot of CVs obtained using Cell 1 with 1 mM of HHQ in the DCE phase while changing [LiCl] in the aqueous phase. The positive and negative limits of the PPW decrease with increasing [LiCl], peak 1 shows little to no change; therefore, peak 1 is likely HHQ facilitated proton transfer. Moreover, as the aqueous phase supporting electrolyte is changed from Li_3(citrate) to Li_2SO_4, NaCl, KCl, and $MgCl_2$ (see Figure 3), the positive potential limit decreases according to the cation present. However, the H^+-HHQ signal (peak 1) returns in the absence of citrate buffer. Therefore, the observed reduction in the PPW at positive potentials is the result of interfacial complexation through eq. 1 between HHQ and the supporting electrolyte cation, in this case Li^+, Na^+, K^+, and Mg^{2+}.

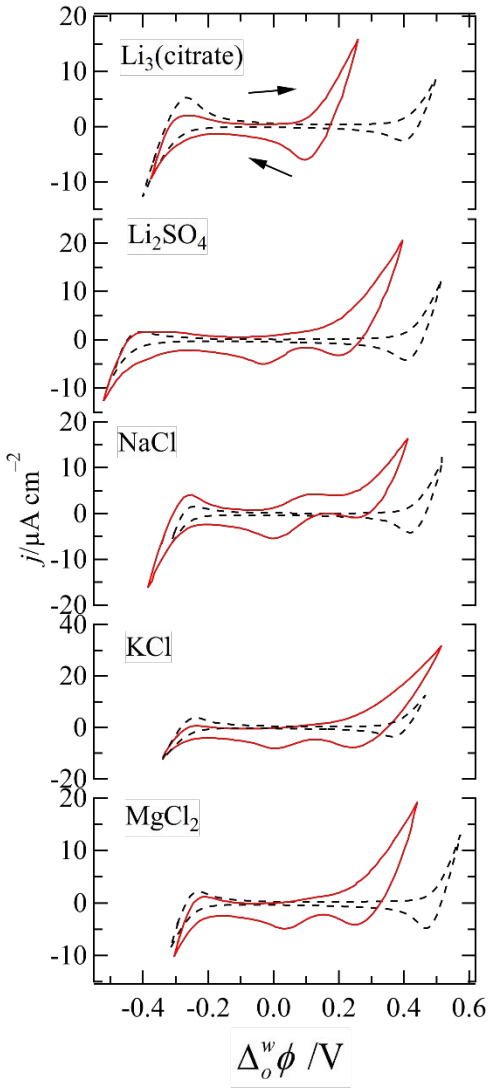

Figure 3. Red solid curves are CVs recorded using Cell 2 with the aqueous phase supporting electrolyte indicated inset, 1 mM HHQ in the organic phase, and v = 25 mV·s^{-1}. Black dashed traces are the same electrolytic cell with no HHQ added – blank curves.

The applied Galvani potential difference between w and o ($\phi_w - \phi_o = \Delta_o^w\phi$) is localized across the ITIES and is the driving force for ion transfer.[39-41] Ligand assisted ion transfer mitigates the amount of applied potential required to induce ion transfer;[39] at the same time, the onset potential is a qualitative indication of metal-ion-ligand binding affinity, such that coordination strength of HHQ to the tested cations can be ranked from highest to lowest as: $H^+ > Na^+ > Li^+ > K^+ \approx Mg^{2+}$.

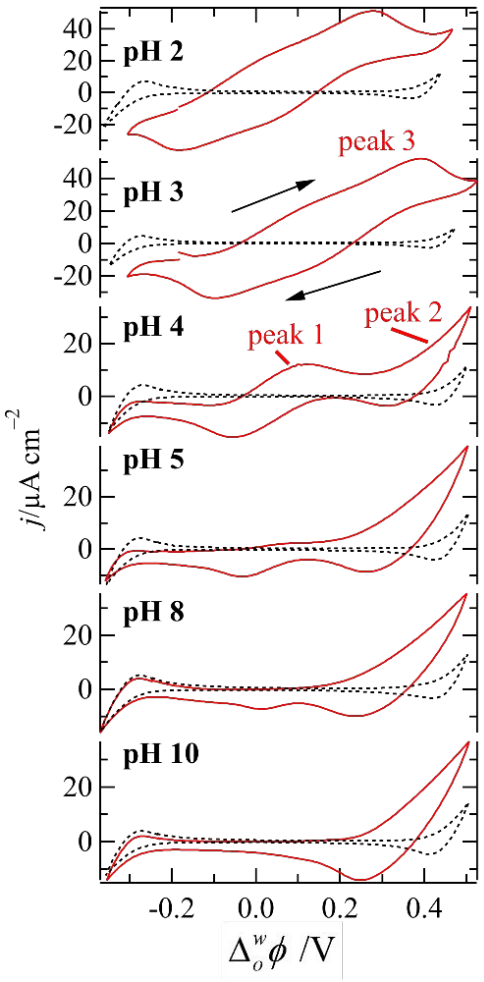

Figure 4. Recorded CVs employing Cell 3 or 4 with 1 mM HHQ in DCE, and varying the aqueous pH as indicated inset using either HCl or LiOH in the aqueous phase. Dotted traces were recorded in the absence of HHQ. All other experimental details are the same as described for Figure 2.

An analytical solution for the thermodynamics of concentration and potential dependent liquid|liquid interfacial complexation was derived by the groups of Mareček and Samec;[55,56] Senda and Kakiuchi;[57] as well as Girault.[43] Based on these analytical solutions, the overall complexation constant (β) and ligand stoichiometry (n in eq. 1) for a TIC/TOC mechanism can be quantitatively determined through,

$$-\frac{zF}{RT}\ln\left(\Delta_o^w\phi_{1/2,ML_n^+} - \Delta_o^w\phi_{M^+}^{o'}\right) = \ln\beta + n\ln\left(c_L^*\right) \qquad [2]$$

where the initial ligand concentration (c_L^*, such that L is HHQ or PQS) is in excess of the initial metal ion or proton (M^+) concentration.[43] $\Delta_o^w\phi_{1/2,ML_n^+}$ is the measured half-wave potential for facilitated ion transfer obtained from the i-V curve and $\Delta_o^w\phi_{M^+}^{o'}$ is the formal metal ion/proton transfer, which is a constant analogous to the formal redox potential at a solid electrode.[39,51,52,58] $\Delta_o^w\phi_{H^+}^{o'}$ is assumed to be 0.580 V[51] unless otherwise noted. The coefficients z, F, R, and T in eq. 2 have their usual significance. Examining eq. 2 closely reveals that it is a linear relationship between

$\Delta_o^w\phi_{1/2,ML_n^+}$ and c_L^* with a slope n, the ligand stoichiometry, and y-intercept proportional to β.[43] β is related to individual complexation constants through,[43]

$$K_j = \frac{c_{ML_n^{z+},\alpha}}{c_{ML_{(n-1)}^{z+},\alpha} c_{L,\alpha}}$$

or,

$$\beta_n = \frac{c_{ML_n^{z+},\alpha}}{c_{M^{z+},\alpha}\left(c_{L,\alpha}\right)^n} = \prod_{k=0}^{n} K_{k,\alpha} \qquad [3]$$

where α is the initial phase – w or o.

In order to quantify the coordination/binding affinity of HHQ to H^+, Cell 3 or 4 was first used which maintained [HHQ] = 1 mM in the DCE phase while varying the aqueous phase pH with either [HCl] or [LiOH], respectively. As the pH is increased to >8 (Figure 4), peak 1 diminishes and eventually disappears (pH = 9-10); while if the pH is decreased (<4, Figure 4), then the current densities of peaks 1 and 2 increase and a third peak emerges. These results at low pH indicate a complex mechanism with multiple stoichiometry's or pathways; however, this is beyond the scope of the present work.

Instead, this work focuses on data obtained using Cell 1 and varying the initial/bulk concentration of HHQ in the DCE phase while the pH was maintained at ~5. Figure 5A is an overlay plot of i-V response recorded when [HHQ] was varied from 10 µM to 2 mM. As the concentration of HHQ was increased, peak 1 and 2 overlap in the CV response (Figure 5A) and the two signals are difficult to differentiate. Therefore, differential pulse voltammetry (DPV) was employed in order to deconvolute the two peak signals (Figure 5B). DPV and similar pulse techniques have been invaluable at ITIES in resolving seemingly overlapping analyte signals; e.g., for the detection of oligopeptides[59], Cr(VI) facilitated ion transfer,[60] simple ion transfer of metal cations limiting the PPW,[52,58] as well as differential pulse stripping voltammetry for ion sensing.[61] The DPV experimental protocol included a potentiostatic pulse that was applied for 20 s at the initial potential. Afterwards, the DPV was initiated with the following parameters: a step potential of 5 mV, modulation amplitude of 100 mV, modulation time of 0.3 s, and interval time of 0.6 s.

The half-wave potential for HHQ facilitated proton transfer from the DPV trace was calculated using eq. 4,[62-64]

$$\Delta_o^w\phi_{max} = \Delta_o^w\phi_{1/2,ML_n^+} + \frac{RT}{zF}\ln\sqrt{\frac{D_w}{D_o}} + \frac{\Delta E}{2} \qquad [4]$$

where $\Delta_o^w\phi_{max}$ is the potential at the peak or maximum current; D_w and D_o are the diffusion coefficients in either phase; and ΔE is the pulse or modulation amplitude. For simplicity $D_w \approx D_o$ and the middle term can be eliminated.

Figure 5C is a plot of $-zF/RT\left(\Delta_o^w\phi_{H\text{-}HHQ_n^+,1/2} - \Delta_o^w\phi_{H^+}^{o'}\right)$ *versus* $\ln[c_{HHQ}]$ utilising $\Delta_o^w\phi_{H\text{-}HHQ_n^+,1/2}$ obtained from eq. 4 for both the forward (●) and reverse (▲) scans in the DPV experiments depicted in Figure 5B. Owing to the slight

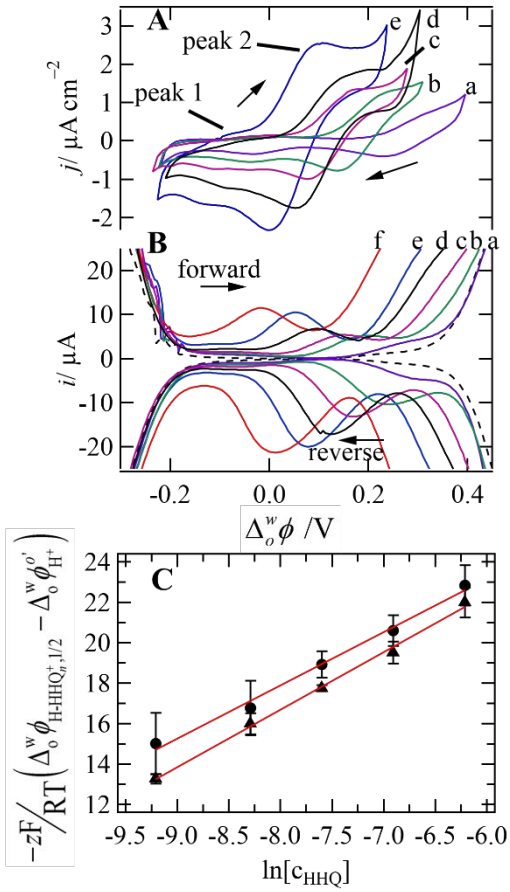

Figure 5: [A] CVs and **[B]** DPVs recorded using Cell 1 with X = [HHQ] = 10 µM-2 mM (traces a-f); the black dashed curve in B is Cell 1 without HHQ added. See the main text for DPV parameters; CV parameters are the same as described for Figure 2. **[C]** $-zF/RT\left(\Delta_o^w\phi_{H\text{-}L_n^+,1/2} - \Delta_o^w\phi_{H^+}^{o'}\right)$ versus ln[c_{HHQ}] from eq. 2, where $\Delta_o^w\phi_{H\text{-}L_n^+,1/2}$ was obtained from the forward (●) and reverse (▲) DPV traces in B. Red traces were obtained from linear regression analysis of the experimental data with Pearson's R values of 0.996 and 0.998, respectively.

deviation in the calculated $\Delta_o^w\phi_{H\text{-}HHQ_n^+,1/2}$ between the two scan directions both were analyzed and then each data set was treated using linear regression analysis (red traces in Figure 5C) which demonstrated excellent fitting with respective Pearson's R values of 0.996 and 0.998 as well as slopes of 2.63 and 2.84 or $n \approx 3$. The intermediate n values may indicate a mixed process with 2-3 HHQ molecules participating while tending towards n = 3; this relatively high n value is likely owing to the large excess [HHQ] relative to that of [H^+] for ligand concentrations >10 µM. The respective y-intercepts for the forward and reverse scans were 38.9 and 39.1, which translate to β's equal to 0.8±0.2 and 1.4±0.3×10^{17}. These results are within the expected error of roughly ±0.005V from the potentiometric measurement and are in good agreement. These β values are similar to phospholipid assisted proton transfer at a w|$CHCl_3$ micro-ITIES.[42] In that report, the phospholipid 1,2-dimyristoyl-sn-glycero-3-phosphocholine (DMPC) was

shown to coordinate in two discreet 1:1, DMPC:H+ facilitated ion transfer steps with overall binding affinities of 1.3×10^{13} and 3.3×10^{8}. The β values determined here are several orders of magnitude higher owing to the higher ordered nature (increased stoichiometry) of the reaction.

Next, using Cells 3 and 4 the electrochemical behavior of PQS was investigated. Figure S3 (see ESI) illustrates the effect of changing the aqueous phase pH with 1 mM PQS dissolved in the organic phase. At pH 4 and 5 one symmetric peak-shaped wave was observed with a half-wave potential at roughly 0.240 V. As the pH increases the peak-shaped wave disappears; therefore, this peak signal is PQS facilitated proton transfer. At pH 3 or lower, the *i*-V curve becomes more convoluted, similar to the HHQ case, with an elongated signal which stretches from ~0.1 to 0.5V. This response is likely 3 discreet events overlapping. Again, for simplicity this is beyond the scope of the present work and in the same manner as HHQ, the H^+-PQS coordination was characterized by maintaining an aqueous phase at pH 5 and varying [PQS].

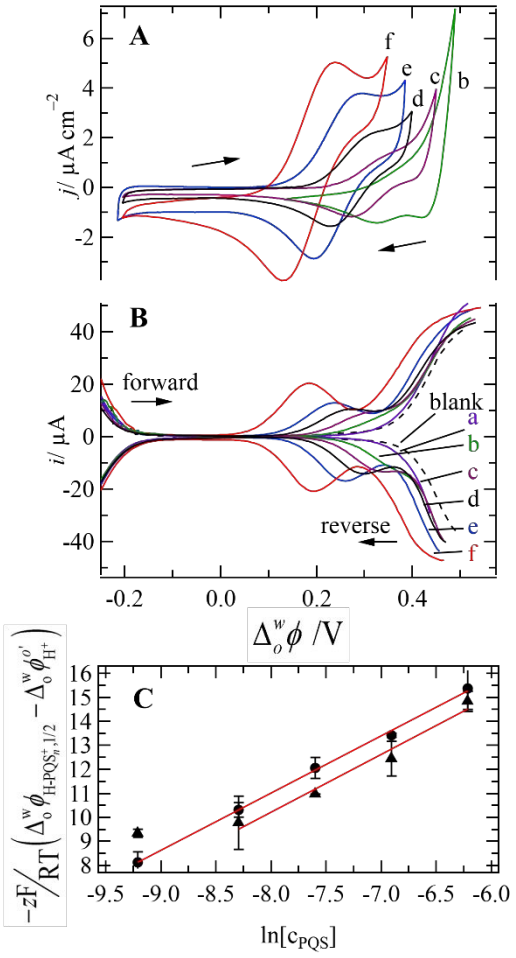

Figure 6: [A] CVs and **[B]** DPVs recorded using Cell 3 with X = [PQS] = 10μM-2mM for traces a-f. All instrument parameters are the same as for those given for Figure 5. **[C]** $-zF/RT\left(\Delta_o^w\phi_{H\text{-}L_n^+,1/2}-\Delta_o^w\phi_{H^+}^{o'}\right)$ versus ln[c_{PQS}] from eq. 2, where $\Delta_o^w\phi_{H\text{-}L_n^+,1/2}$ was obtained from the forward (●) and reverse (▲) DPV traces in B. Red traces were obtained from linear regression analysis of the experimental data with Pearson's R values of 0.999 and 0.987, respectively.

Figure 6A and B detail the CV and DPV responses, respectively, using Cell 3 with [PQS] varied from 10 μM-2 mM. The H^+-PQS half-wave potential ($\Delta_o^w\phi_{H\text{-}PQS_n^+,1/2}$) was obtained from the forward and reverse DPV traces (Figure 6B) and the $-zF/RT\left(\Delta_o^w\phi_{H\text{-}PQS_n^+,1/2}-\Delta_o^w\phi_{H^+}^{o'}\right)$ *versus* ln[c_{PQS}] relationship has been plotted in Figure 6C. Similar to the HHQ DPV experiments, $\Delta_o^w\phi_{H\text{-}PQS_n^+,1/2}$ was calculated using eq. 4. Owing to the H^+-PQS response being close to the positive PPW limit, there was a higher degree of error associated with determining $\Delta_o^w\phi_{H\text{-}PQS_n^+,1/2}$ for the reverse DPV scan. This lead to a relatively poor fit of the linear regression with a Pearson's R = 0.953 for the reverse scan *versus* R = 0.999 for the forward scan. Therefore, a linear fitting neglecting the lowest [PQS] data-point was performed providing an R = 0.987. In this way, a slope or *n* = 2.39 and 2.40 was obtained for the forward and reverse scans, respectively; *i.e.*, $n \approx 2$. Next, *y*-intercept's of 30.1 and 29.4 or $\beta = 1.2$ and 0.6×10^{13} were obtained for the respective forward and reverse scans. These data suggest that HHQ has a higher binding affinity for protons than PQS. Proton binding by PQS would be inhibited by the proton already bound to the nitrogen in PQS (Figure 1) but would also be enhanced by the presence of an electron-donating – *via* resonance stabilization – hydroxyl group at the 3-position (Figure 1). The hydroxyl group para to the nitrogen in HHQ is also electron donating courtesy of resonance stabilization, however, since the nitrogen is deprotonated it is not sterically hindered.

pK_{a1} and pK_{a2} values of 3.02/3.43 and 11.46/9.89, respectively, for HHQ/PQS have been calculated by Zhou *et al.*[49] using Marvin 6.8, ChemAxon software. Owing to the multiple and different HHQ- and PQS-proton coordination stoichiometry, it is difficult to make direct comparisons; however, the overall binding affinities for HHQ and PQS follow the same trend as observed by Zhou *et al.*[49] and in this way agree qualitatively. The presence of lithium may also constitute interference; however, this is likely quite small considering the relatively low pK_a's or high proton binding affinities already reported.

Conclusions

The thermodynamics of *P. aeruginosa* QS metabolites, HHQ and PQS, coordination with protons as well as alkali and alkali earth metal ions through a facilitated ion transfer mechanism across a w|DCE interface have been elucidated. The HHQ- and PQS-proton assisted transfer revealed high ligand:proton stoichiometry's of 3:1 and 2:1, respectively, that is likely owing to the relatively high ligand concentrations employed. These results provide insight into the interaction of these small molecules with multiple dissolved cations indicating the powerful Lewis acid character of QS molecules.

Because this type of electrochemical detection method does not depend on the redox activity of the target charged species, this study acts as a proof-of-concept for the detection of other QS molecules and pathogenic bacteria. Moreover, this method exploits the ability of HHQ, PQS, and

other QS molecules to chelate cations, as well as their natural hydrophobicity. Work is currently under way to exploit the latter by extracting HHQ and PQS to the organic phase from either Artificial Sputum Medium (ASM) or patient sputum samples, followed by electrochemical detection as described herein. Furthermore, with this method, a micro-pipette probe can be utilized incorporating an organic solvent or hydrophobic ionic liquid impregnated membrane separating the ASM or patient sputum from an internal acidic aqueous phase. In this way, the QS molecule would partition to the organic phase and then undergo electrochemically monitored facilitated ion transfer to the internal aqueous phase. Thus, a *point-of-care-device* or even *in vivo* electrochemical monitoring probe could be employed as a sensor to detect the QS molecules in patient sputum. However, this is beyond the scope of the present work.

ASSOCIATED CONTENT

Supporting Information

CVs employing Cell 1 with 1 mM HHQ and varying either the scan rate or [LiCl] in the aqueous phase. CVs employing Cell 3 with 1 mM PQS and varying the pH of the aqueous phase. The Supporting Information is available free of charge on the ACS Publications website.

AUTHOR INFORMATION

Corresponding Author

* tstockmann@mun.ca
* micheal.scanlon@ul.ie

Author Contributions

The manuscript was written through contributions of all authors. All authors have given approval to the final version of the manuscript.

ACKNOWLEDGMENT

This publication has emanated from research by M. D. S. and A. F. M. -O. supported by the European Research Council through a Starting Grant (agreement no. 716792) and in part by a research grant from Science Foundation Ireland (SFI) (grant number 13/SIRG/2137). E. D. B. acknowledges funding received from an Irish Research Council Government of Ireland Postgraduate Scholarship Award (grant number GOIPG/2016/1217). GMG acknowledges funding from the Irish Research Council and SFI (12/IP/1315, 12/TIDA/B2405 and 12/RC/2275). T.J.S. acknowledges funding from an NSERC Discovery Grant (#2019-06074) and Discovery Launch Supplement. The authors thank Dr Rafael Cano for providing a sample of PQS.

ABBREVIATIONS

ITIES: interface between two electrolytic solutions; w: water; o: oil; DCE: 1,2-dichloroethane; HHQ: 4-hydroxy-2-heptylquinoline; *P. aeruginosa*: *Pseudomonas aeruginosa*; PQS: Pseudomonas quinolone signal; AHQ:2-Alkyl-4-quinolones; HAQ: 4-hydroxy-2-alkylquinolines; QS: quorum sensing; TIC: transfer through interfacial ion complexation; TOC: transfer followed by organic phase complexation.

REFERENCES

(1) Bassler, B. L.; Losick, R. Bacterially speaking. *Cell* **2006**, *125*, 237-246.

(2) Simoska, O.; Sans, M.; Fitzpatrick, M. D.; Crittenden, C. M.; Eberlin, L. S.; Shear, J. B.; Stevenson, K. J. Real-time electrochemical detection of Pseudomonas aeruginosa phenazine metabolites using transparent carbon ultramicroelectrode arrays. *ACS Sensors* **2019**, *4*, 170-179.

(3) Stevens, A. M.; Schuster, M.; Rumbaugh, K. P. Working together for the common good: Cell-cell communication in bacteria. *J. Bacteriol.* **2012**, *194*, 2131.

(4) Fletcher, M. P.; Diggle, S. P.; Crusz, S. A.; Chhabra, S. R.; Cámara, M.; Williams, P. A dual biosensor for 2-alkyl-4-quinolone quorum-sensing signal molecules. *Environ. Microbiol.* **2007**, *9*, 2683-2693.

(5) Engebrecht, J.; Nealson, K.; Silverman, M. Bacterial bioluminescence: Isolation and genetic analysis of functions from Vibrio fischeri. *Cell* **1983**, *32*, 773-781.

(6) Fuqua, C.; Greenberg, E. P. Self Perception in bacteria: quorum sensing with acylated homoserine lactones. *Current Opinion in Microbiology* **1998**, *1*, 183-189.

(7) Déziel, E.; Lépine, F.; Milot, S.; He, J.; Mindrinos, M. N.; Tompkins, R. G.; Rahme, L. G. Analysis of *Pseudomonas aeruginosa* 4-hydroxy-2-alkylquinolines (HAQs) reveals a role for 4-hydroxy-2-heptylquinoline in cell-to-cell communication. *Proc. Natl. Acad. Sci* **2004**, *101*, 1339-1344.

(8) Kåhrström, C. T. Entering a post-antibiotic era? *Nature Reviews Microbiology* **2013**, *11*, 146.

(9) Bukelman, O.; Amara, N.; Mashiach, R.; Krief, P.; Meijler, M. M.; Alfonta, L. Electrochemical analysis of quorum sensing inhibition. *Chem. Commun.* **2009**, 2836-2838.

(10) Sismaet, H. J.; Pinto, A. J.; Goluch, E. D. Electrochemical sensors for identifying pyocyanin production in clinical Pseudomonas aeruginosa isolates. *Biosens. Bioelectron.* **2017**, *97*, 65-69.

(11) Sismaet, H. J.; Banerjee, A.; McNish, S.; Choi, Y.; Torralba, M.; Lucas, S.; Chan, A.; Shanmugam, V. K.; Goluch, E. D. Electrochemical detection of Pseudomonas in wound exudate samples from patients with chronic wounds. *Wound Rep. Reg.* **2016**, *24*, 366-372.

(12) Bjarnsholt, T.; Kirketerp-Møller, K.; Jensen, P. Ø.; Madsen, K. G.; Phipps, R.; Krogfelt, K.; Høiby, N.; Givskov, M. Why chronic wounds will not heal: a novel hypothesis. *Wound Repair and Regeneration* **2008**, *16*, 2-10.

(13) Sismaet, H. J.; Goluch, E. D. Electrochemical probes of microbial community behavior. *Annu. Rev. Anal. Chem.* **2018**, *11*, 441-461.

(14) Santiveri, C. R.; Sismaet, H. J.; Kimani, M.; Goluch, E. D. Electrochemical detection of Pseudomonas aeruginosa in polymicrobial environments. *ChemistrySelect* **2018**, *3*, 2926-2930.

(15) Li, S.; Mou, Q.; Feng, N.; Leung, P. H. M. A selective medium for pyocyanin-dependent fast electrochemical detection of Pseudomonas aeruginosa in environmental microbial samples. *Int. J. Electrochem. Sci.* **2018**, *13*, 3789-3798.

(16) Kuss, S.; Amin, H. M. A.; Compton, R. G. Electrochemical detection of pathogenic bacteria—recent strategies, advances and challenges. *Chemistry: An Asian Journal* **2018**, *13*, 2758-2769.

(17) Darch Sophie, E.; Koley, D. Quantifying microbial chatter: scanning electrochemical microscopy as a tool to study interactions in biofilms. *Proceedings of the Royal Society A: Mathematical, Physical and Engineering Sciences* **2018**, *474*, 20180405.

(18) Whiteley, M.; Diggle, S. P.; Greenberg, E. P. Progress in and promise of bacterial quorum sensing research. *Nature* **2017**, *551*, 313.

(19) Oziat, J.; Gougis, M.; Malliaras, G. G.; Mailley, P. Electrochemical characterizations of four main redox–metabolites of Pseudomonas aeruginosa. *Electroanalysis* **2017**, *29*, 1332-1340.

(20) Elliott, J.; Simoska, O.; Karasik, S.; Shear, J. B.; Stevenson, K. J. Transparent carbon ultramicroelectrode arrays for the electrochemical detection of a bacterial warfare toxin, pyocyanin. *Anal. Chem.* **2017**, *89*, 6285-6289.

(21) Buzid, A.; Reen, F. J.; Langsi, V. K.; Muimhneacháin, E. Ó.; O'Gara, F.; McGlacken, G. P.; Luong, J. H. T.; Glennon, J. D. Direct and

rapid electrochemical detection of Pseudomonas aeruginosa quorum signaling molecules in bacterial cultures and cystic fibrosis sputum samples through cationic surfactant-assisted membrane disruption. *ChemElectroChem* **2017**, *4*, 533-541.

(22) Burkitt, R.; Sharp, D. Submicromolar quantification of pyocyanin in complex biological fluids using pad-printed carbon electrodes. *Electrochem. Commun.* **2017**, *78*, 43-46.

(23) Buzid, A.; Shang, F.; Reen, F. J.; Muimhneacháin, E. Ó.; Clarke, S. L.; Zhou, L.; Luong, J. H. T.; O'Gara, F.; McGlacken, G. P.; Glennon, J. D. Molecular signature of Pseudomonas aeruginosa with simultaneous nanomolar detection of quorum sensing signaling molecules at a boron-doped diamond electrode. *Sci. Reports* **2016**, *6*, 30001.

(24) Bellin, D. L.; Sakhtah, H.; Zhang, Y.; Price-Whelan, A.; Dietrich, L. E. P.; Shepard, K. L. Electrochemical camera chip for simultaneous imaging of multiple metabolites in biofilms. *Nature Communications* **2016**, *7*, 10535.

(25) Alatraktchi, F. A. a.; Johansen, H. K.; Molin, S.; Svendsen, W. E. Electrochemical sensing of biomarker for diagnostics of bacteria-specific infections. *Nanomedicine* **2016**, *11*, 2185-2195.

(26) Seviour, T.; Doyle, L. E.; Lauw, S. J. L.; Hinks, J.; Rice, S. A.; Nesatyy, V. J.; Webster, R. D.; Kjelleberg, S.; Marsili, E. Voltammetric profiling of redox-active metabolites expressed by Pseudomonas aeruginosa for diagnostic purposes. *Chem. Commun.* **2015**, *51*, 3789-3792.

(27) Webster, T. A.; Sismaet, H. J.; Conte, J. L.; Chan, I. p. J.; Goluch, E. D. Electrochemical detection of Pseudomonas aeruginosa in human fluid samples via pyocyanin. *Biosens. Bioelectron.* **2014**, *60*, 265-270.

(28) Kim, E.; Leverage, W. T.; Liu, Y.; White, I. M.; Bentley, W. E.; Payne, G. F. Redox-capacitor to connect electrochemistry to redox-biology. *Analyst* **2014**, *139*, 32-43.

(29) Connell, J. L.; Kim, J.; Shear, J. B.; Bard, A. J.; Whiteley, M. Real-time monitoring of quorum sensing in 3D-printed bacterial aggregates using scanning electrochemical microscopy. *Proc. Natl. Acad. Sci* **2014**, *111*, 18255-18260.

(30) Bellin, D. L.; Sakhtah, H.; Rosenstein, J. K.; Levine, P. M.; Thimot, J.; Emmett, K.; Dietrich, L. E. P.; Shepard, K. L. Integrated circuit-based electrochemical sensor for spatially resolved detection of redox-active metabolites in biofilms. *Nature Communications* **2014**, *5*, 3256.

(31) Zhou, L.; Glennon, J. D.; Luong, J. H. T.; Reen, F. J.; O'Gara, F.; McSweeney, C.; McGlacken, G. P. Detection of the Pseudomonas Quinolone Signal (PQS) by cyclic voltammetry and amperometry using a boron doped diamond electrode. *Chem. Commun.* **2011**, *47*, 10347-10349.

(32) Vukomanovic, D. V.; Zoutman, D. E.; Marks, G. S.; Brien, J. F.; van Loon, G. W.; Nakatsu, K. Analysis of pyocyanin from Pseudomonas aeruginosa by adsorptive stripping voltammetry. *J. Pharmacol. Toxicol. Methods* **1996**, *36*, 97-102.

(33) Fletcher, M. P.; Diggle, S. P.; Cámara, M.; Williams, P. Biosensor-based assays for PQS, HHQ and related 2-alkyl-4-quinolone quorum sensing signal molecules. *Nature Protocols* **2007**, *2*, 1254.

(34) Diggle, S. P.; Matthijs, S.; Wright, V. J.; Fletcher, M. P.; Chhabra, S. R.; Lamont, I. L.; Kong, X.; Hider, R. C.; Cornelis, P.; Cámara, M.; Williams, P. The Pseudomonas aeruginosa 4-quinolone signal molecules HHQ and PQS play multifunctional roles in quorum sensing and iron entrapment. *Chem. Biol.* **2007**, *14*, 87-96.

(35) Cernat, A.; Tertis, M.; Gandouzi, I.; Bakhrouf, A.; Suciu, M.; Cristea, C. Electrochemical sensor for the rapid detection of Pseudomonas aeruginosa siderophore based on a nanocomposite platform. *Electrochem. Commun.* **2018**, *88*, 5-9.

(36) Monzó, J.; Insua, I.; Fernandez-Trillo, F.; Rodriguez, P. Fundamentals, achievements and challenges in the electrochemical sensing of pathogens. *Analyst* **2015**, *140*, 7116-7128.

(37) Koley, D.; Ramsey, M. M.; Bard, A. J.; Whiteley, M. Discovery of a biofilm electrocline using real-time 3D metabolite analysis. *Proc. Natl. Acad. Sci* **2011**, *108*, 19996-20001.

(38) Leipert, J.; Bobis, I.; Schubert, S.; Fickenscher, H.; Leippe, M.; Tholey, A. Miniaturized dispersive liquid-liquid microextraction and MALDI MS using ionic liquid matrices for the detection of bacterial communication molecules and virulence factors. *Anal. Bioanal. Chem.* **2018**, *410*, 4737-4748.

(39) Peljo, P.; Girault, H. H. In *Encyclopedia of Analytical Chemistry*; John Wiley & Sons, Ltd: 2012.

(40) Scanlon, M. D.; Smirnov, E.; Stockmann, T. J.; Peljo, P. Gold nanofilms at liquid–liquid interfaces: an emerging platform for redox electrocatalysis, nanoplasmonic sensors, and electrovariable optics. *Chem. Rev.* **2018**, *118*, 3722-3751.

(41) Herzog, G. Recent developments in electrochemistry at the interface between two immiscible electrolyte solutions for ion sensing. *Analyst* **2015**, *140*, 3888-3896.

(42) Stockmann, T. J.; Noel, J.-M.; Abou-Hassan, A.; Combellas, C.; Kanoufi, F. Facilitated Lewis Acid Transfer by phospholipids at a (water|$CHCl_3$) liquid|liquid interface towards biomimetic and energy applications. *J. Phys. Chem. C* **2016**, *120*, 11977–11983.

(43) Reymond, F.; Lagger, G.; Carrupt, P.-A.; Girault, H. H. Facilitated ion transfer reactions across oil|water interfaces. Part II. Use of the convoluted current for the calculation of the association constants and for an amperometric determination of the stoichiometry of MLjz+ complexes. *J. Electroanal. Chem.* **1998**, *451*, 59-76.

(44) Stockmann, T. J.; Angelé, L.; Brasiliense, V.; Combellas, C.; Kanoufi, F. Platinum nanoparticle impacts at a liquid|liquid interface. *Angew. Chem. Int. Ed.* **2017**, *56*, 13493-13497.

(45) Stockmann, T. J.; Lu, Y.; Zhang, J.; Girault, H. H.; Ding, Z. Interfacial complexation reactions of Sr^{2+} with octyl(phenyl)-N,N-diisobutylcarbamoylmethylphosphine oxide for understanding its extraction in reprocessing spent nuclear fuels. *Chem. Eur. J.* **2011**, *17*, 13206-13216.

(46) Shioya, T.; Nishizawa, S.; Teramae, N. Complexation kinetics of 8-quinolinol derivatives with Ni(II) and Zn(II) at the 1,2-dichloroethane–water interface as studied by electrolyte ascending electrode polarography. *Langmuir* **1999**, *15*, 2575-2579.

(47) Shioya, T.; Nishizawa, S.; Teramae, N. Complexation kinetics of 5-alkyloxymethyl-8-quinolinols at liquid–liquid interfaces as studied by dynamic interfacial tensiometry. *Langmuir* **1998**, *14*, 4552-4558.

(48) McGlacken, G. P.; McSweeney, C. M.; O'Brien, T.; Lawrence, S. E.; Elcoate, C. J.; Reen, F. J.; O'Gara, F. Synthesis of 3-halo-analogues of HHQ, subsequent cross-coupling and first crystal structure of Pseudomonas quinolone signal (PQS). *Tetrahedron Lett.* **2010**, *51*, 5919-5921.

(49) Zhou, L.; Reen, F. J.; O'Gara, F.; McSweeney, C. M.; Clarke, S. L.; Glennon, J. D.; Luong, J. H. T.; McGlacken, G. P. Analysis of pseudomonas quinolone signal and other bacterial signalling molecules using capillaries coated with highly charged polyelectrolyte monolayers and boron doped diamond electrode. *J. Chromatogr. A* **2012**, *1251*, 169-175.

(50) Zhou, M.; Gan, S.; Zhong, L.; Dong, X.; Ulstrup, J.; Han, D.; Niu, L. Improvement in the assessment of direct and facilitated ion transfers by electrochemically induced redox transformations of common molecular probes. *Phys. Chem. Chem. Phys.* **2012**, *14*, 3659-3668.

(51) Olaya, A. J.; Méndez, M. A.; Cortes-Salazar, F.; Girault, H. H. Voltammetric determination of extreme standard Gibbs ion transfer energy. *J. Electroanal. Chem.* **2010**, *644*, 60-66.

(52) Stockmann, T. J.; Montgomery, A.-M.; Ding, Z. Determination of alkali metal ion transfers at liquid|liquid interfaces stabilized by a micropipette. *J. Electroanal. Chem.* **2012**, *684*, 6-12.

(53) Torralba, E.; Molina, A.; Serna, C.; Ortuno, J. A. Rigorous characterization of the Facilitated Ion Transfer at ITIES in normal pulse voltammetry. Comparison with the approximated treatments. *Int. J. Electrochem. Sci.* **2012**, *7*, 6771-6786.

(54) In *CRC Handbook of Chemistry and Physics, 99th Edition*; Rumble, J. R., Ed.; CRC Press/Taylor & Francis: Boca Raton, FL., 2018.

(55) Homolka, D.; Holub, K.; Mareček, V. Facilitated ion transfer across the water/nitrobenzene interface. Theory for single-scan voltammetry applied to a reversible system. *J. Electroanal. Chem. Interfacial Electrochem.* **1982**, *138*, 29-36.

(56) Samec, Z.; Homolka, D.; Mareček, V. Charge transfer between two immiscible electrolyte solutions. Part VIII. Transfer of alkali and alkaline earth-metal cations across the water/nitrobenzene interface facilitated by synthetic neutral ion carriers. *J. Electroanal. Chem. Interfacial Electrochem.* **1982**, *135*, 265-283.

(57) Kakiuchi, T.; Senda, M. Current-potential curves for facilitated ion transfer across oil/water interfaces in the presence of successive complex formation. *J. Electroanal. Chem.* **1991**, *300*, 431-445.

(58) Stockmann, T. J.; Montgomery, A.-M.; Ding, Z. Formal transfer potentials of strontium and uranyl ions at water|1,2-dichloroethane interfaces. *Can. J. Chem.* **2012**, *90*, 836-842.

(59) Scanlon, M. l. D.; Herzog, G. g.; Arrigan, D. W. M. Electrochemical detection of oligopeptides at silicon-fabricated micro-liquid|liquid interfaces. *Anal. Chem.* **2008**, *80*, 5743-5749.

(60) O'Mahony, A. M.; Scanlon, M. D.; Berduque, A.; Beni, V.; Arrigan, D. W. M.; Faggi, E.; Bencini, A. Voltammetry of chromium(VI) at the liquid|liquid interface. *Electrochem. Commun.* **2005**, *7*, 976-982.

(61) Strutwolf, J.; Scanlon, M. D.; Arrigan, D. W. M. The performance of differential pulse stripping voltammetry at micro-liquid-liquid interface arrays. *J. Electroanal. Chem.* **2010**, *641*, 7-13.

(62) Girault, H. *Analytical and Physical Electrochemistry*; 1st ed.; EPFL Press: Lausanne, CH, 2004.

(63) Scholz, F. Voltammetric techniques of analysis: the essentials. *ChemTexts* **2015**, *1*, 17.

(64) Stojek, Z. In *Electroanalytical methods. Guide to experiments and applications.*; Scholz, F., Ed.; Springer: Berlin, 2010, p 107.

TOC Graphic

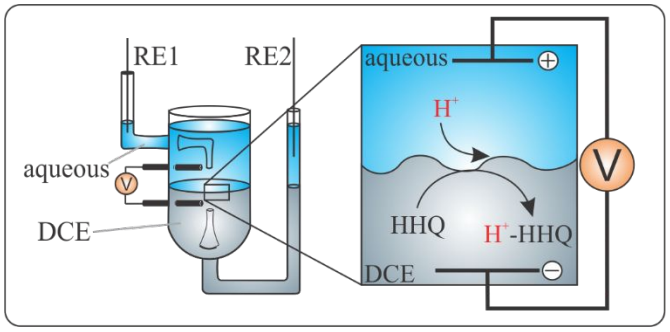

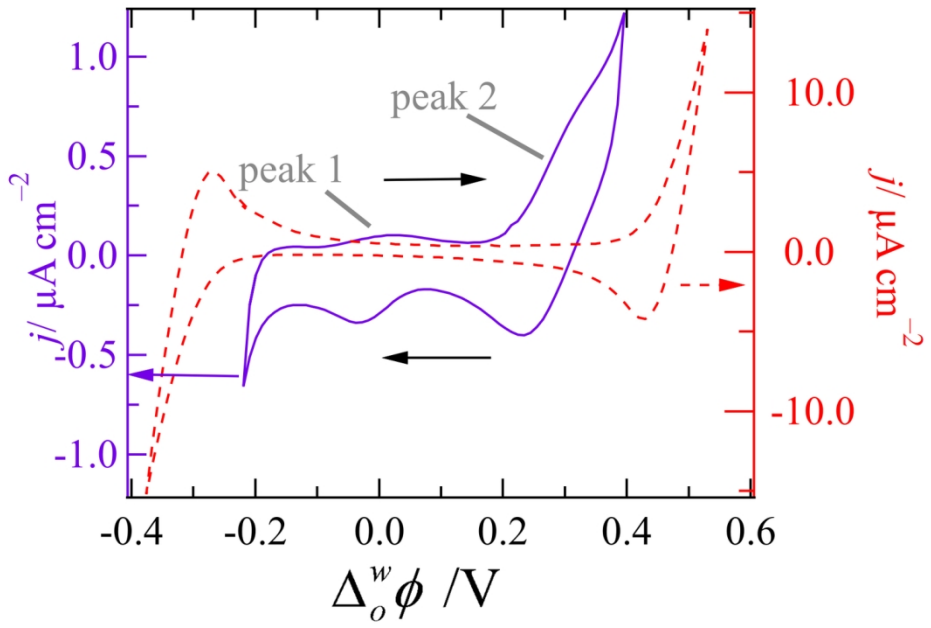

Figure 2

138x99mm (300 x 300 DPI)

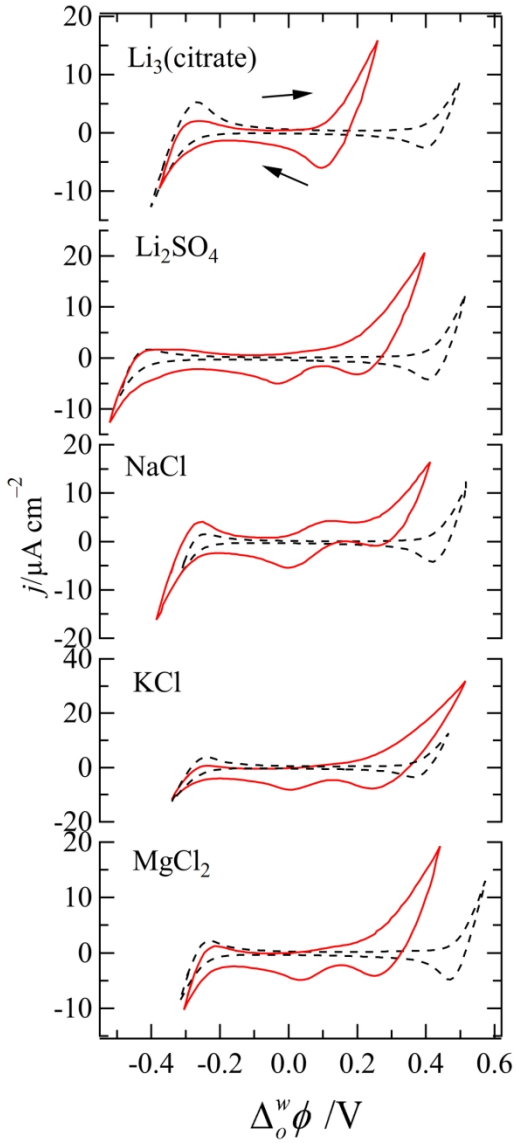

Figure 3

106x215mm (300 x 300 DPI)

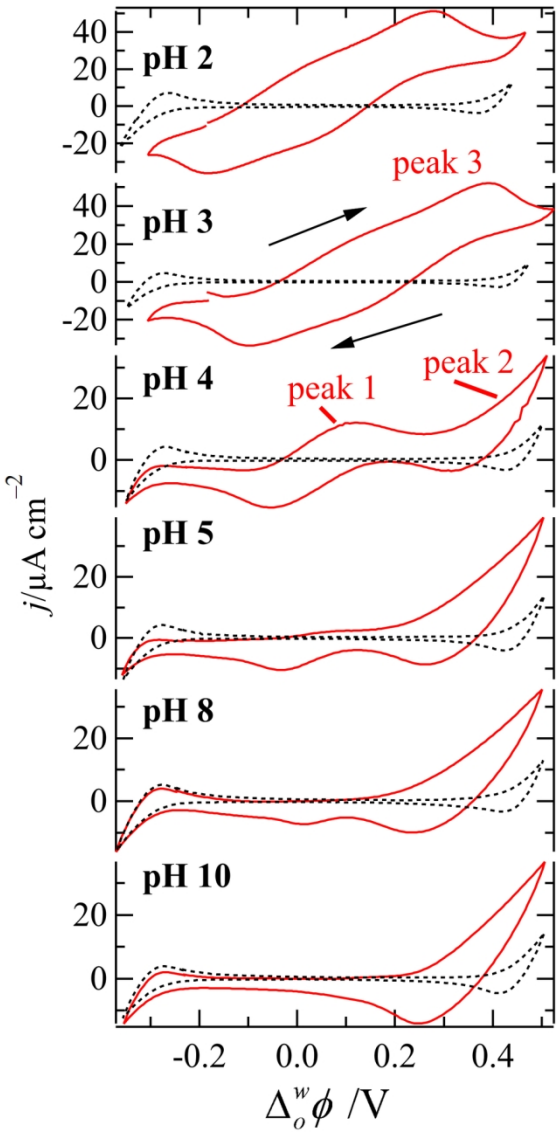

Figure 4

101x183mm (300 x 300 DPI)

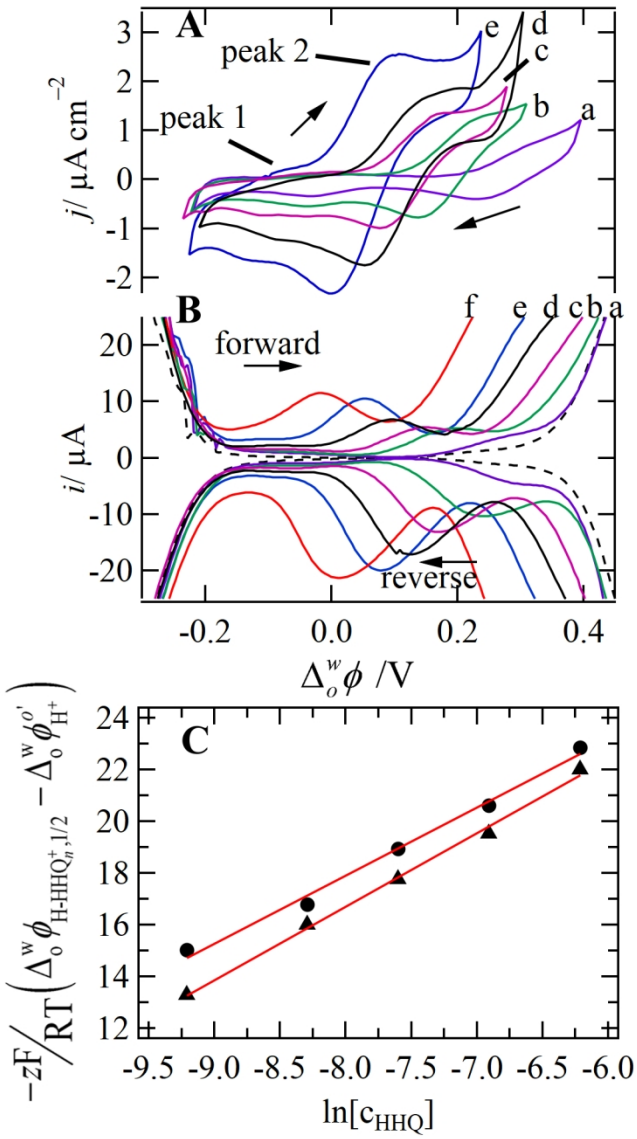

Figure 5

111x188mm (288 x 288 DPI)

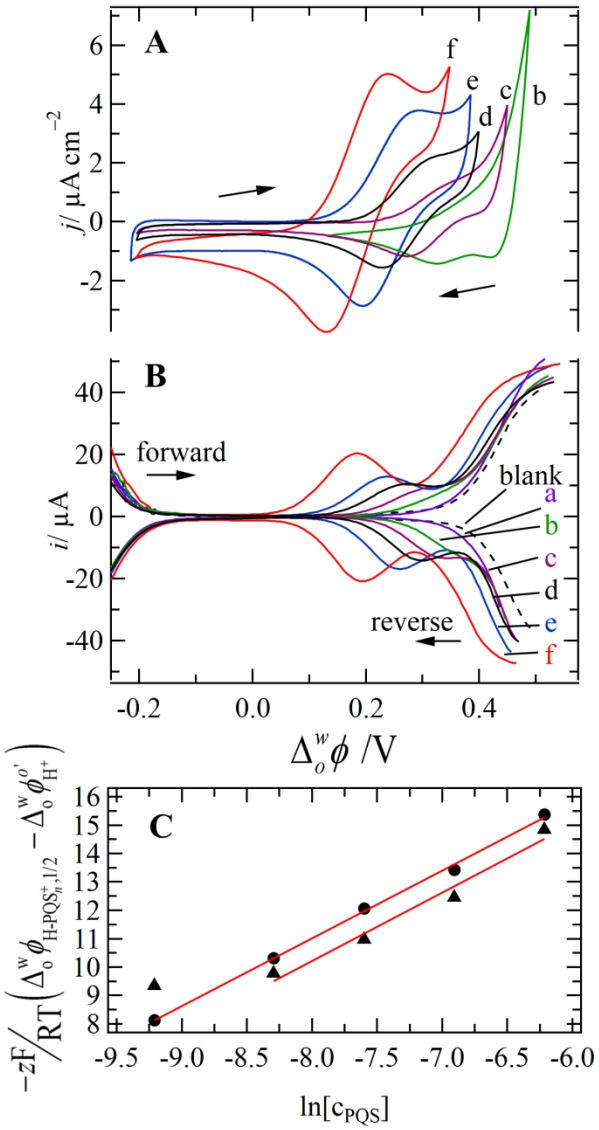

Figure 6

121x221mm (288 x 288 DPI)